Differences between observed and a coupled simulation of North Atlantic sea surface currents and temperature

Robert L. Molinari,[1,2,3] Zulema Garraffo,[1] and Derrick Snowden[3,4]

[1] North Atlantic sea surface temperature (SST) distributions derived from observations and a coupled model from NOAA's Geophysical Fluid Dynamics Laboratory, CM2.1, are compared to evaluate the model's ability to simulate recent (1900 to the present) oceanic surface characteristics. The North Atlantic focus will limit our analyses to spatial scales less than gyre, scales usually not addressed in previous model-observation comparisons. Identifying model differences from observations at these scales will assist modelers in identifying problems to be considered and remedies to be applied. The properties compared are the mean annual SST, standard deviation, amplitude of the annual and semiannual harmonic, decadal meridional movements of the axis of the Gulf Stream, propagation of SST anomalies along the axis of the Gulf Stream, and 100-year trends in SST records. Because of the dependence of SST on surface currents, observed flow from surface drifters and simulated flow from 15 m fields are also compared. The model simulates the large-scale properties of all the variables compared. However, there are areas of differences in some variables that can be related to inadequacies in the simulated current fields. For example, the model Gulf Stream (GS) axis after separation from the western boundary is located some 100 km north of the observed axis, which contributes to an area of warmer simulated SSTs. The absence of a slope current in the same region that advects colder water from the Labrador Sea in the observations also contributes to this area of higher model SSTs. The model North Atlantic Current (NAC) is located to the east of the observed NAC contributing to a large area of SST discrepancy. The patterns of the amplitude of the annual harmonic are similar with maximum amplitude off the east coast of northern North America. The semiannual harmonic exhibits relatively large amplitudes (>1°C) north of about 55°N, a signal not found in the observations. In both the model and observations, a region of increased standard deviations encompasses the GS and NAC. The model simulates north-south migrations of the GS core but at a longer period (20 years) than observed. The model does not simulate the SST anomalies that propagate along the observed GS and NAC. The model captures both the spatial and temporal characteristics of the Atlantic Multidecadal Oscillation. Both model and observations exhibit a dipole in trends, with positive trends in the subtropical Atlantic and negative trends in the subpolar gyre. The modeled region of negative trends is limited to the western subpolar Atlantic. The observed trends extend farther to the east.

1. Introduction

[2] The Geophysical Fluid Dynamics Laboratory (GFDL) of the National Oceanic and Atmospheric Administration develops coupled global general circulation models (GCM) that are used "for the study of weather and climate" [*Delworth et al.*, 2006]. The evaluation of the capability of these models to simulate accurately the present global air-sea-land climate is one step in the evolution of these GCMs toward climate and ecological forecasting applications. Thus, in addition to describing the formulation of GFDL's newest global coupled models, CM2.0 and 2.1, *Delworth et al.* [2006] and *Gnanadesikan et al.* [2006] also provide comparisons of simulation results with observations. Com-

[1]Rosenstiel School of Marine and Atmospheric Science, University of Miami, Coral Gables, Florida, USA.

[2]Cooperative Institute for Marine and Atmospheric Studies, Miami, Florida, USA.

[3]Atlantic Oceanographic and Meteorological Laboratory, National Oceanic and Atmospheric Administration, Miami, Florida, USA.

[4]Now at Climate Project Office, Office of Climate Observations, National Oceanic and Atmospheric Administration, Silver Spring, Maryland, USA.

parisons already completed show that on North Atlantic basin scales the models satisfactorily reproduce large-scale phenomena. *Delworth et al.* [2006] also find that CM2.1 proves to be an improvement over CM2.0 in simulating most observations compared and thus version CM2.1 will be addressed in this paper.

[3] *Knutson et al.* [2006] have compared representations of sea surface temperature (SST) characteristics derived from CM2 model results with those derived from in situ observations. They find that on basin spatial scales, over the past 130 years, various properties of the model SST fields such as mean global temperature, standard deviations, spectra, etc. compare favorably with observed fields. *Knutson et al.* [2006] also compared model and observed SST characteristics from a few smaller regions. However, these regional studies provided limited details on the accuracy of the SST simulations.

[4] Previous studies have demonstrated that SST signals in the area encompassing the subtropical and subpolar gyres of the North Atlantic can play an important role in atmospheric climate and ecosystem evolution. Thus, herein we compare in greater detail than previously attempted results from GFDL model CM2.1 with observed North Atlantic SST variability on several timescales. We will follow the philosophy used by *Smith et al.* [2000] in their comparison of one model with two different resolutions with observations. However, we will concentrate on smaller than global scales. Specifically, we will concentrate on the largest regional differences between simulation and observations in order to identify aspects of the model where more in depth study is needed to resolve the divergences. We recognize the difficulties inherent in trying to correct model deficiencies when the model's resolution is of the same magnitude as the features considered. However, comparison efforts such as presented here must be the first step in developing predictive models. Unfortunately, the next step, resolving discrepancies is beyond the scope of the present study but is strongly encouraged.

[5] The structure of this paper is as follows. We begin with a description of CM2.1 and the in situ observations used in the comparisons. It has been demonstrated that the majority of the largest model-observation mean SST differences can be related to the differences in average simulated and observed surface currents of the region [*Delworth et al.*, 2006]. Thus, mean surface currents are also described and used as the primary foundation for studying SST differences. Comparisons of several temporal SST features are then provided. We conclude with a discussion of the strengths and weaknesses of CM2.1 in simulating modes of the present SST (i.e., past 100+ years) climate of the North Atlantic.

2. Coupled Model and Observations

[6] The model results analyzed in this paper are from the GFDL GCM CM2.1 climate simulation for the period 1861–2000. This coupled model is composed of separate atmosphere, land, sea ice and ocean components, which are joined by a "coupler" that passes fluxes between the various model components. The model analyzed here use different gas and aerosol conditions from years 1860 to 2000. The control simulation uses the 1860 gas and aerosol conditions.

[7] No flux corrections are applied in the simulation. The ocean model has a nominal grid spacing of 1° in longitude and meridional grid spacing decreasing from 1° in midlatitude to 1/3° near the equator. The vertical structure of the water column is approximated by 50 levels of varying thickness, with 10 m thickness in the top 220 m. Updates in the ocean model from earlier geophysical fluid dynamics models can be found in the paper by *Griffies et al.* [2005]. Additional details are given in the paper by *Knutson et al.* [2006] and for the ocean model in the paper by *Gnanadesikan et al.* [2006].

[8] The 1861–2000 CM2.1 simulations consist of an ensemble of five members. Each ensemble is initialized by conditions from states separated by at least 40 years in a multicentury control run. We typically examined three of the five members but in view of their similarities, we limit all our analysis to one member, except for the discussion of the Atlantic Multidecadal Oscillation (AMO) and trends where all five members are used.

[9] The Extended Reconstruction SST (ERSST) data set of *Smith and Reynolds* [2003, 2004] is used to compare with model results. ERSST combines satellite observations and 1856 to 2002 in situ data to generate monthly SST fields on a 2° grid. *Smith and Reynolds* [2003] claim a 95% confidence uncertainty in a near global average of 0.1°C after 1950. However, they do note that regional differences in uncertainties do exist related to data availability, surface fronts, etc. We use only the 100-year record extending from 1900 to 1999 in our analyses.

[10] *Rayner et al.* [2003] performed a careful analysis of SST and sea ice to generate the Hadley Center for Climate Prediction and Research climatology, HadISSTY1. Methods for generating the climatologies were different than used by *Smith and Reynolds* [2003] but the data used were similar (i.e., Comprehensive Ocean-Atmosphere Data Set (COADS) for a portion of the in situ observations). They compared results from ERSST with those from HadISSTY1. Largest differences in the North Atlantic were in the vicinity of the Gulf Stream and were of the order 1°C. They attribute the differences to "different analysis resolutions."Away from intense currents and the northern North Atlantic, maximum absolute differences are less than 0.4°C. This favorable comparison provides some confidence in using ERSST while providing a crude uncertainty of 0.4°C in this data set.

[11] Since surface currents play an important role in establishing SST patterns, a comparison of observed and simulated surface flow is also provided. The observed regional velocity distribution (Figure 1) is taken from a 1° of latitude by 1° of longitude climatology of surface currents derived from satellite tracked surface drifters. The drifter data record extends from 1992 through 2005. The drifters are nominally coupled to the flow at 15 m by a holey sock drogue. The derivation of the climatology is given in the paper by *Lumpkin and Garraffo* [2005] and the data are available on www.aoml.noaa.gov/phod/dac/drifter_climatology.html. The second level of the model is also centered at 15 m and model data from this depth are used for comparison with the observations.

3. Comparison of Modeled and Observed Mean Annual Surface Current and SST Properties

[12] Several other papers have recently compiled drifter data to generate sea surface climatologies of the North
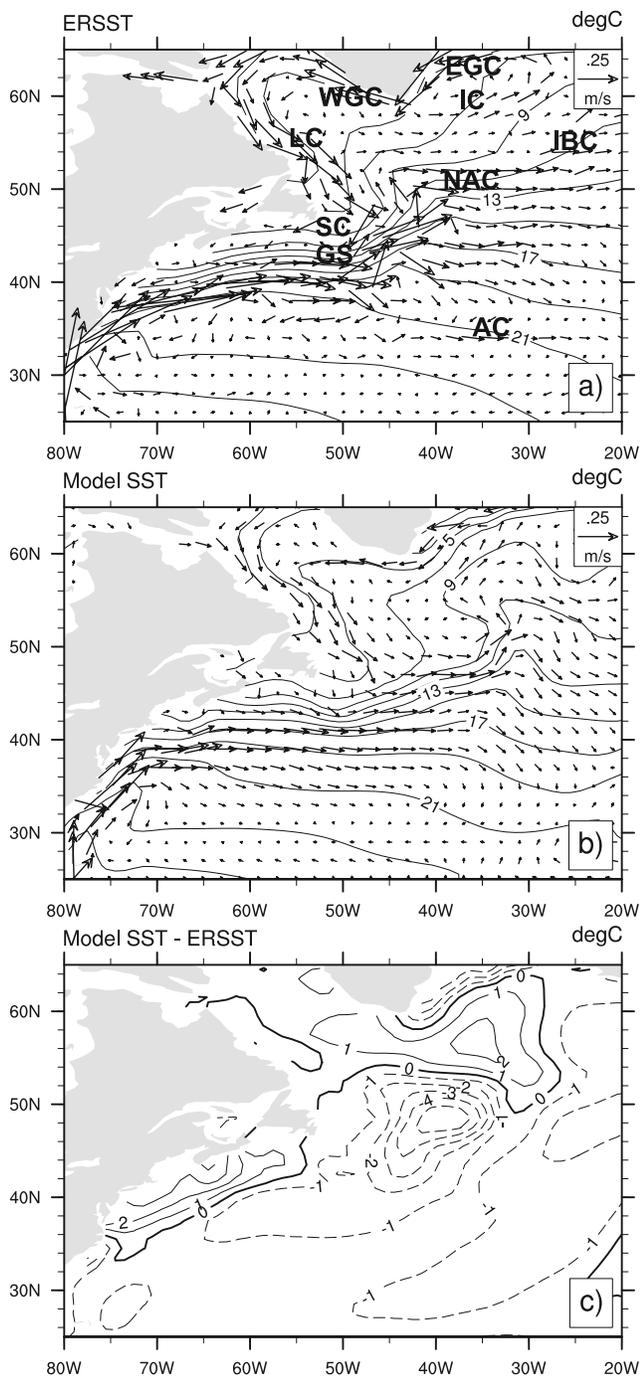
Figure 1. (top) Observed mean surface currents (1992–2005), derived from surface drifters drogued at 15 m, and sea surface temperature (SST) (°C) distributions. Currents are truncated from a 1° latitude-longitude grid to a 2° to increase clarity. SC, slope current; GS, Gulf Stream; AC, Azores Current; NAC, North Atlantic Current; E(W)GC, East (West) Greenland Current; LC, Labrador Current; IC, Irminger Current; IBC, Iceland Basin Current (middle) Simulated mean surface current, from the model depth at 15 m, and SST (°C). (bottom) Simulated minus observed SST distribution (°C).

Atlantic, typically north of 40°N where coverage is extensive [*Fratantoni*, 2001; *Reverdin et al.*, 2003, *Flatau et al.*, 2003, *Brambilla and Talley*, 2006]. Although using the same raw drifter data, the times of data collection and the analyses techniques used are frequently different. However, major circulation features are similar. Descriptions of circulation from these papers will serve to corroborate the comparison presented herein. Our range of interest extends from 20°N to 70°N, thus including the central and northern subtropical gyre and the entire subpolar gyre, Figure 1.

[13] We recognize the potential problems in comparing a 14-year observational record with a 100-year model simulation (e.g., the presence of strong decadal signals). As a zero-order evaluation of the comparison of the model and observed currents, the model was subsampled for the 10-year period (1990–2000). The comparison results from this shorter model climatology are consistent with those from the 100-year run (e.g., in both, unrealistic eastward displacement of the northward flowing North Atlantic Current (NAC), and eastward extension of the Gulf Stream).

[14] The area encompassed in Figure 1 displays similar distributions in model-observations SST differences as in the paper by *Delworth et al.* [2006] although they use a different SST climatology. Specifically, in the extreme south of the grid (22°N to 26°N), which includes the North Equatorial Current, simulated currents are consistently northward (Figure 1). The observed currents are more variable, possibly related to data density. In this region and extending northward to about 35°N, SST differences are of the order 1°C, with the model exhibiting a "cold bias." *Delworth et al.* [2006] also compare results from CM2.1 to a "Reynolds" analysis. The results are very similar [*Delworth et al.*, 2006, Figure 2] with model-observation differences of the order 1°C in the subtropics.

[15] *Delworth et al.* [2006] find that the easterlies in the Trade Wind region of CM2.1 are greater than observed [*Delworth et al.*, 2006, Figure 22]. These enhanced easterlies through Ekman effects could be responsible for the northward flow on the southern boundary of the grid (Figure 1). However, since the northward flow would tend to transport warmer water from the south, these currents could only reduce the cold bias at these latitudes and not cause it. *Delworth et al.* [2006] attribute the cold discrepancy to a negative bias in the model's absorption of shortwave radiation (the latter defined as the difference between downward minus upward shortwave radiation at the top of the atmosphere).

[16] Farther north in the subtropical gyre, the dominant circulation feature in both the observations and model is the Gulf Stream (GS). As with most coarse resolution, noneddy resolving models, the simulated GS separates from the boundary at a more northerly latitude (40°N) than observed (37°N), Figure 2. After leaving the boundary, both simulated and observed GS then turn eastward with the axis of the former located some 100 km north of the latter (Figure 1). In addition in this area the model underestimates the core speeds of the GS.

[17] In the region after separation, the observed GS is bounded on the north by the slope current (SC) (Figure 2). The SC appears as a continuation of the Labrador Current, LC, which flows inshore of the GS around the Tail of the Grand Banks, then westward to the mid-Atlantic bight,
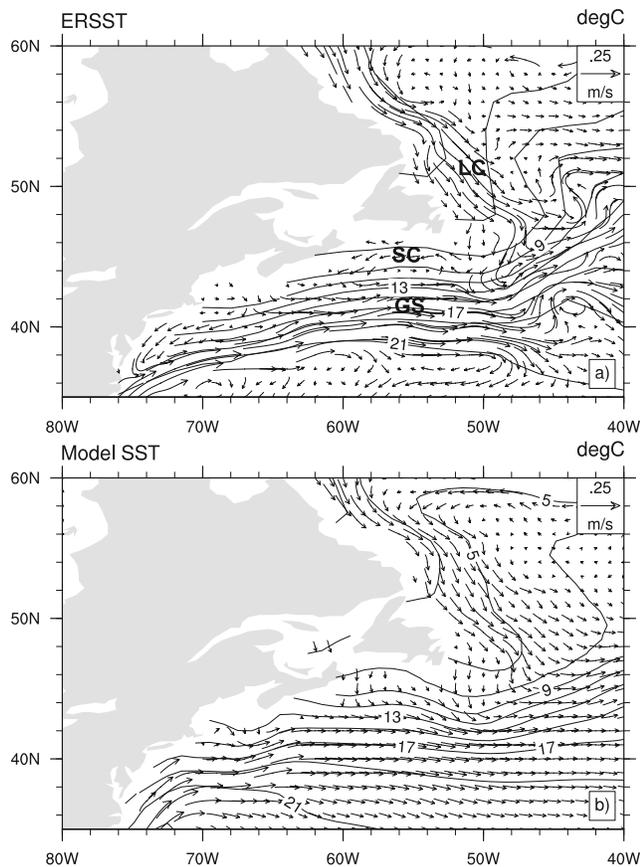
Figure 2. (top) Observed and (bottom) simulated SST (°C) and surface current distributions from the area of the separation latitude of the Gulf Stream. Current indicators are the same as in Figure 1.

Figure 2. In contrast, however, *Fratantoni* [2001] notes, "while the mean surface field is suggestive of such a connection, horizontal resolution and data density on the southern periphery of the Grand Banks is insufficient to reveal a continuous surface flow between the two regions."

[18] In the model, the LC joins the GS to flow eastward with none of the flow curving anticyclonically to the west. Thus, the model does not simulate a SC. Assuming there is a connection in the observed mean LC and SC flows, the latter would transport colder subpolar waters westward (Figure 2). The absence of the SC in the simulations can thus contribute to the 3°C difference in temperature north of the observed GS (Figure 1). In addition, the 100 km northerly position of the modeled GS axis relative to the observed axis can also contribute to the higher model temperatures found north of the Stream.

[19] Flowing eastward, the observed GS begins to bifurcate into northern and southern components at about 50°W. The southern branch turns back to the west, with westward flow centered at about 36°N, representing the southern recirculation gyre of the GS. In contrast, the simulated GS continues considerably farther eastward to about 35°W before splitting. Although a portion of the flow turns southward at this longitude, westward flow is not found until south of 30°N, implying a different spatial structure for the simulated southern recirculation gyre, to be discussed shortly.

[20] East of 40°W between about 34°N and 36°N the observations depict the Azores Current. This surface intensified eastward flow does not appear in the simulation. *Smith et al.* [2000] compare two ocean-only simulations of the North Atlantic one with a 0.1° horizontal resolution and the other with a 0.28° resolution. In the former simulation the Azores Current is fed by both the GS and the NAC and is characterized by strong eddies and meanders. The Azores Current is not simulated in the 0.28° model nor CM2.1, suggesting that its absence may be related to the poorer resolution of these two simulations.

[21] Model temperatures are less than observed in the region of simulated southeastward flow and observed eastward flow. The model SST contours dip somewhat to the south in the area of the observed Azores Current. This cooling could be related to advection by the extension of the NAC, which provides the source for the southeastward flow after crossing the mid-Atlantic ridge (Figure 1).

[22] The observed subpolar gyre exhibits a more complicated structure than the subtropical gyre probably because its dynamics are not purely Sverdrupian [*Bryan et al.*, 1995]. *Reverdin et al.* [2003], using surface drifters, indicate that the subpolar gyre has 2 parts, an eastern part that serves as a conduit of Atlantic waters from the south to the Norwegian Sea and a western part that is characterized by a well defined cyclonic gyre. *Fratantoni* [2001] and *Flatau et al.* [2003] provide similar descriptions of the circulation in the subpolar North Atlantic, as does the representation of observed flow in Figure 1.

[23] The western gyre has similar components in both the model and observations, but the details of the individual currents are sufficiently different to cause dramatic SST offsets. The observed GS turns cyclonically around the Grand Banks and flows northeastward to about 43°W before turning eastward as the NAC. In contrast, before turning north, the simulated GS continues farther eastward to about 35°W where it bifurcates at the model's version of the mid-Atlantic ridge (Figure 1). Thus, the observed NAC flows north, west of the simulated NAC (Figure 1). The large separation in the positions of the northward flow of the NAC (observed 43°W versus simulated 35°W) contributes to the 4°C temperature difference centered at about 47°N, 40°W (Figure 1).

[24] As noted by *Reverdin et al.* [2003] several current components diverge from the NAC when it flows eastward. One component of the NAC is the Irminger Current (IC), which flows northward along the western side of the Reykjanes Ridge both in observations and model (Figure 1). The axis of the observed IC (30°W to 27°W) is located to the east of the simulated IC axis (38°W to 33°W). The connection of the IC to the NAC is also depicted in the drifter compilation of *Treguier et al.* [2005], for example, but not in all the ocean model simulations presented by these authors. The zonal separation of the observed and simulated IC can contribute to the 2°C difference in SST centered at about 57°N, 36°W (Figure 1).

[25] The IC turns cyclonically at the northern extreme of our grid, 66°N. It then flows southwestward to the east of the East Greenland Current (EGC) as shown schematically in the paper by *Fratantoni* [2001]. In the CM2.1 simulation, the model's IC has turned cyclonically at about the same position as observed, before turning to flow south alongside
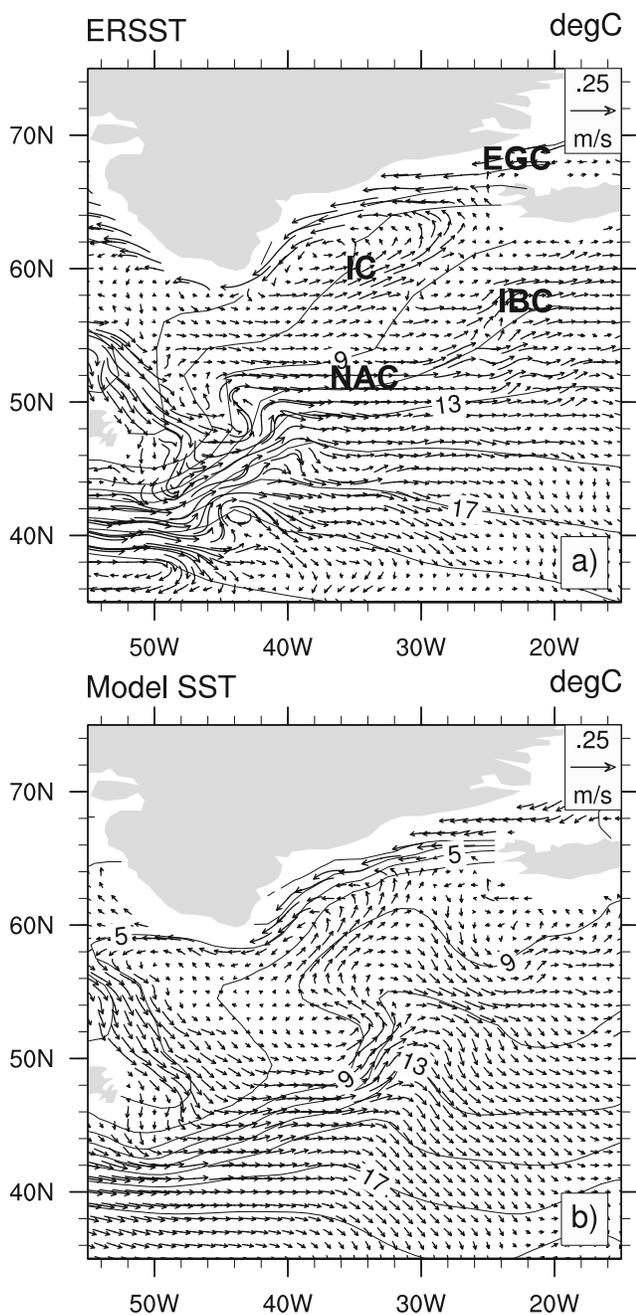
Figure 3. Same as Figure 2, except for the area of the bifurcation of the Gulf Stream. Current identifiers are the same as in Figure 1.

the EGC (Figure 1). The negative SST differences along the east Greenland coast represent a warmer observed than simulated EGC and possibly IC (Figure 1). However, the simulated and modeled EGC and IC are approximately colocated. Thus the cause of this discrepancy is not readily related to differences in model and observed representations of the two flows.

[26] In both representations, the West Greenland Current (WGC) does not appear in the 2° grid figure we adapted for clarity (Figure 1) because of its narrow horizontal extent. However, the separation of the WGC from the boundary appears in both model and observations as westward flow

centered at about 65°W. This flow joins the western boundary LC found in both model and observations (Figure 1). In summary, the model reproduces the major currents of the western subpolar gyre: the eastward flowing NAC, the northward flowing IC, the southward flowing EGC, the northward flowing WGC and the southward flowing LC, with some differences in the actual positions of these flows.

[27] Two branches of the NAC that eventually become the Norway Current characterize the eastern component of the subpolar gyre (Figure 3). The western branch of the northward flow is observed in the middle of the Iceland basin between approximately 54°N and 60°N and 28°W and 21°W in the World Ocean Circulation Experiment drifter climatology generated by *Treguier et al.* [2005]. This flow appears in approximately the same location in our Eulerian climatology but not in the CM2.1 simulation (Figure 3). In the extreme eastern subpolar Atlantic boundary flow is to the northeast feeding the Norway Current (Figure 1).

[28] Finally, there is a large difference between observed and simulated currents between 45°N and 55°N and 20°W and 35°W (Figure 3). In this region the model currents are predominantly southeastward after turning anticyclonically over the model's mid-Atlantic ridge. The observed currents are primarily eastward (i.e., the NAC). The difference in current direction and the waters these currents transport could contribute to the 2°C difference between observed and simulated SST in this region.

4. Characteristics of Time-Dependent SST Signals

4.1. Amplitude of the Semiannual Harmonic (ASAH)

[29] In large areas of the Atlantic the semiannual and annual harmonics compose a large component of the overall variability. Thus to compute interannual variability independent of the effects of externally induced anomalies, the semiannual and annual harmonics are computed from mean monthly grid point values. These harmonics are then removed from the SST at each grid point and standard deviations are then estimated from the total SST records. Semiannual and annual harmonics are also computed to provide an indirect measure of the of the model's ability to simulate accurately simulated surface fluxes at these timescales.

[30] While recognizing that cyclical signals require both amplitude and phase for a complete definition, we follow the reasoning of *Covey et al.* [2000] in their multimodel intercomparison and only address the amplitude of the annual harmonics. Specifically, they note that for air temperature "outside the tropics the seasonal cycle is characterized by a rather uniform phase." We assume a similar characteristic for SST in most areas of the ocean (i.e., away form the tropics, strong currents, etc.) and only consider the amplitudes of the semiannual and annual harmonics.

[31] The observed ASAH distribution is very similar to that generated by *Yashayaev and Zveryaev* [2001], although they used a different analytical approach. Specifically the observed fields are characterized by (1) maximum values along and offshore of the east coast of the northern U.S. and southern Canada (the extreme amplitude of 1.4°C matches the extreme estimated by *Yashayaev and Zveryaev* [2001] in
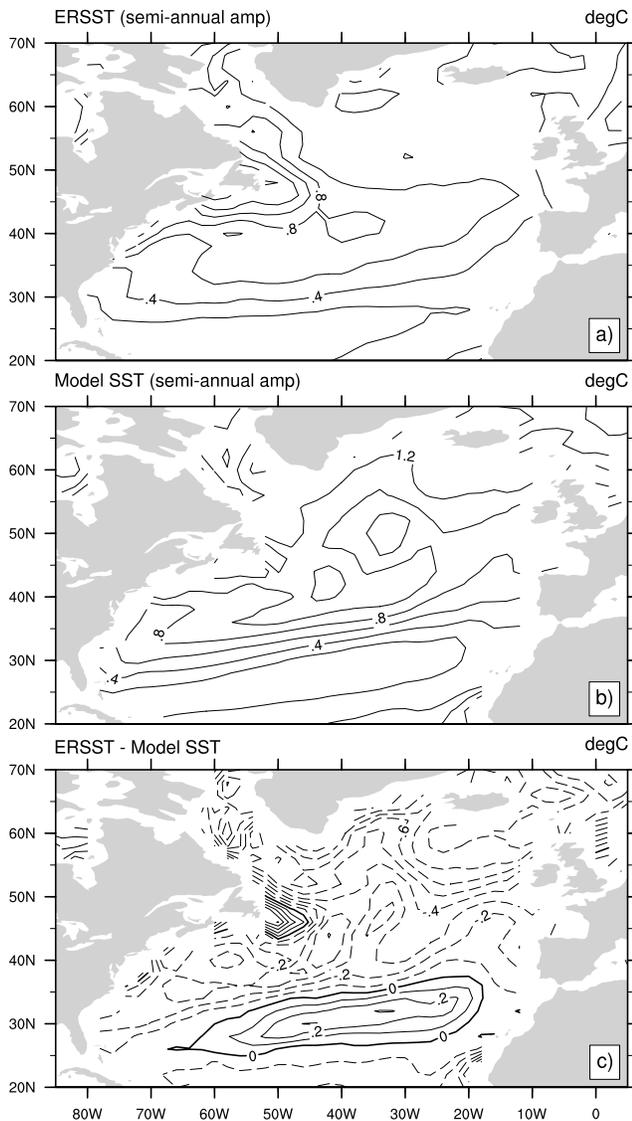
Figure 4. Amplitude of semiannual harmonic: (top) observed (°C), (middle) simulated (°C), and (bottom) observed minus simulated difference between the two representations (°C).

the same region), (2) minimum amplitudes in the extreme northern and southern portions of the grid, and (3) intermediate values in the central subtropical gyre (Figure 4). Simulated fields have similar properties south of 50°N including an eastward-extended area of higher amplitudes at about 40°N.

[32] Throughout most of the basin, the simulated ASAH are larger than the observed ASAH. The only exceptions are (1) a band extending across the basin centered between about 25 °N and 35°N and (2) a coastal region at about 50°N and 50°W. South of 40°N, differences in ASAH typically are less than an absolute value of 0.2°C.

[33] In contrast to observed ASAH, however, the simulated ASAH field increases monotonically poleward of 50°N. The observed ASAH distribution does not increase uniformly in the band north of 50°N, but does increase in the northern Labrador Sea and to the east of southern

Greenland (Figure 4). The *Yashayaev and Zveryaev* [2001] ASAH distribution also does not increase monotonically north of 50°N, placing in question the increase in CM2.1.

4.2. Amplitude of the Annual Harmonic (AAH)

[34] Both the observed and simulated fields of the AAH are characterized by an area of maximum values along and offshore of the east coast of North America (Figure 5), similar to the ASAH fields (the extreme AAH amplitude of 8°C matches the extreme estimated by *Yashayaev and Zveryaev* [2001] in the same region). In both cases, AAH values greater than 4°C extend from approximately 35°N to north of Newfoundland (~54°N, north of the GS). AAH greater than 4°C extend farther east in the simulated than observed field (Figure 5). Although not exactly colocated, there are areas in the extreme southern and northern portions of the basin in both model and observed representations of AAH where amplitudes are less than 2°C.
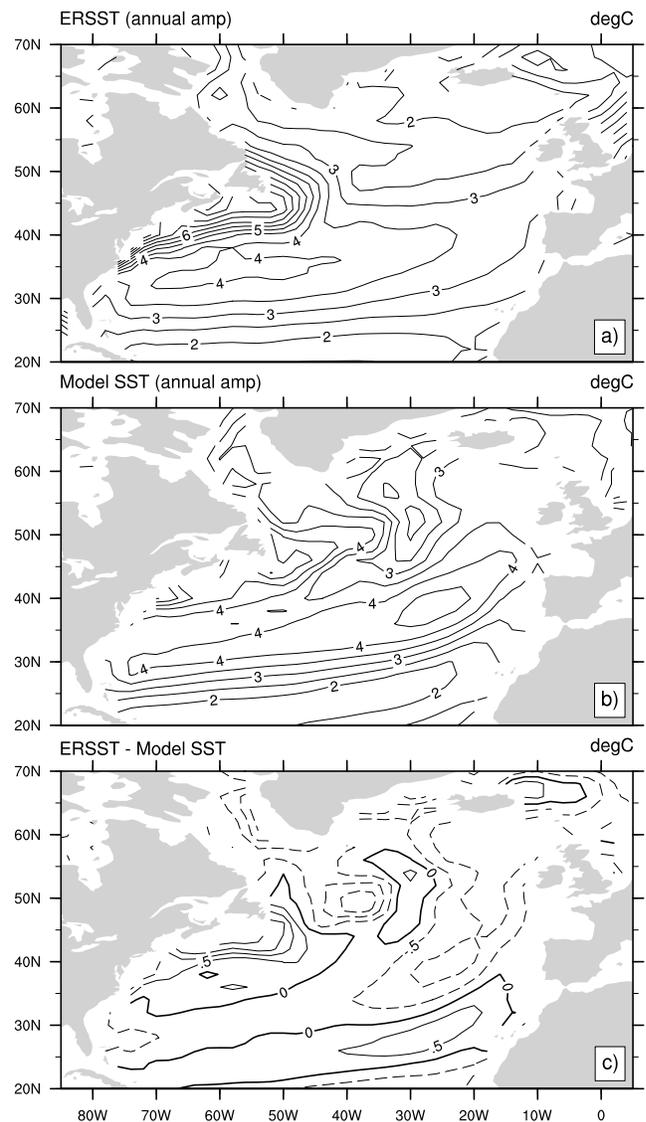

Figure 5. Same as Figure 4, except for amplitude of the annual harmonic.
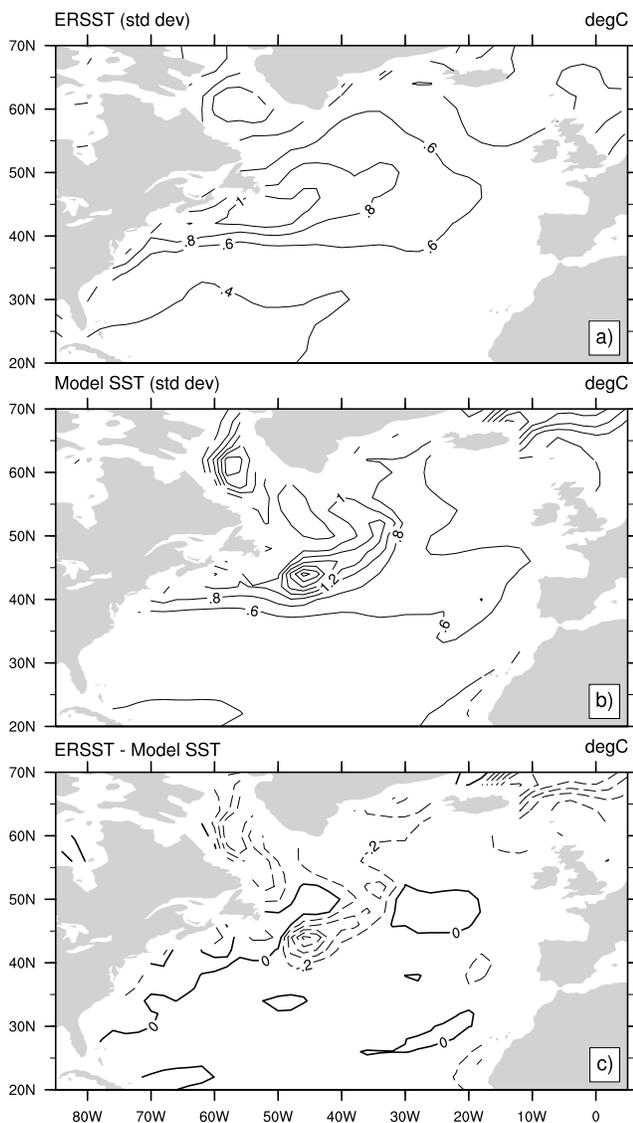
Figure 6. Same as Figure 4, except for standard deviation (°C) of SST time series after the annual signal and trend have been removed from each grid point time series.

Similarly in the midbasin, the values of AAH range from 3°C to greater than 4°C in both observations and model (Figure 5).

4.3. Standard Deviations

[35] Prior to calculation of standard deviations mean monthly SST values (i.e., the annual cycle) and trends are computed at each model and observed grid point and subtracted from the 100 years of SST values. Thus, the standard deviations shown in Figure 6 provide a measure of variability at scales greater than interannual.

[36] The observed standard deviation values are of the order 0.4°C to 0.6°C throughout most of the basin south of 40°N (Figure 6). Observed standard deviations greater than 0.8°C are found along the axis of the GS and NAC and in the central Labrador Sea. Largest standard deviations are located just to the west of where the GS turns northeastward to become the NAC (Figure 3).

[37] The model standard deviation distribution has many similarities to the observed field (Figure 6) including (1) values of about 0.4°C to 0.6°C throughout most of the basin, (2) values greater than 0.8°C along the simulated axis of the GS, (3) largest values just to the west of where the simulated GS turns northeastward to become the NAC (Figure 3), and (4) large values (greater than 1°C) in the central Labrador Sea.

[38] South of about 40°N and east of about 30°W (i.e., away from the boundary currents) model and observed differences are typically less than 0.2°C. *Smith and Reynolds* [2003] give a mean global error for ERSST of 0.1 after 1950 suggesting that the observed and model longer timescale variability is not significantly different. Furthermore, the small differences also imply that in the more quiescent areas of the North Atlantic CM2.1 simulates scales greater than interannual quite accurately.

[39] As described in the previous section, immediately after turning to the northeast, the observed NAC forms to the west of the modeled NAC (Figure 3). Similarly, the area of maximum standard deviation observed in the data is displaced to the west of the maximum in the simulation (Figure 6). This displacement results in differences between observed and simulated standard deviations of the order −0.75°C in the region bounded approximately by 41°N and 45°N and 48°W and 42°W (Figure 6). Large differences (≤0.5°C) between data and model are also observed in the central Labrador Sea, where simulated standard deviations are greater than observed standard deviations (Figure 6).

[40] The structure of the maxima in observed and simulated standard deviation fields are very similar to the eddy kinetic energy (EKE) field computed from drifter velocity data by *Fratantoni* [2001]. A region of high EKEs and standard deviations extends along the axis of the GS and NAC. Maximum EKEs are located along 40°N between about 70°W and 50°W. Maximum observed standard deviations (>1°C) are somewhat to the north and east centered at 45°N between 60°W and 42°W. Maximum simulated SST standard deviations are located at approximately 42°N and 47°W. The modeled maximum SST variability is greater than the observed (Figure 6). The similarity between the observed EKEs and standard deviations in the area of intense currents suggest current induced SST variability.

4.4. Decadal Variability

[41] Several types of observed decadal SST variability related to GS anomalies have been described, which could have climate and ecosystem implications. Two will be discussed here, meridional migrations of the axis of the GS and propagation of SST signals. Because of the intense SST gradients associated with the axis of the GS, order of 100 km meridional shifts in this core can result in 2°C to 4°C changes in SST in the region (Figure 1).

[42] Several studies have observed meridional migrations of the GS using either satellite [e.g., *Taylor and Stephens*, 1998] or in situ observations [e.g., *Joyce et al.*, 2000; *Molinari*, 2004]. *Molinari* [2004] used the trace of the 15°C isotherm at 150 m to represent the speed core of the GS. At this depth, the 15°C isotherm is located in the center of the maximum temperature gradient representative of the GS and thus suitable to represent meridional migration of this inertial flow (Figure 7). The same isotherm at 150 m in
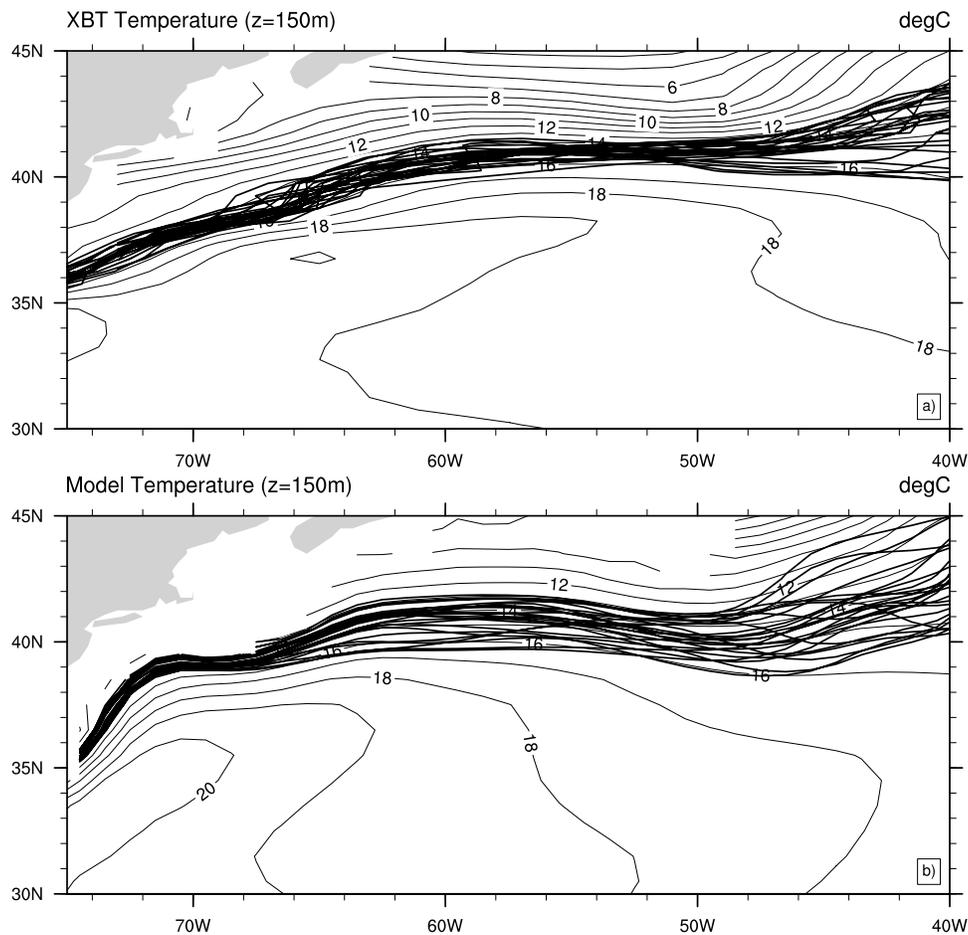
Figure 7. (top) Observed and (bottom) simulated mean annual temperature distribution at 150 m (°C) and the traces of the observed (modeled) 15°C (12°C) isotherms. Every third (fifth) trace is taken from the observations (model).

the model is located on the southern edge of the maximum gradients representative of the simulated core of the GS (Figure 7). Thus, we use the model's position of the 12°C isotherm at 150 m to represent the GS core and meridional migrations of the model GS as it is closer to the maximum temperature gradients representative of the GS core.

[43] To obtain the GS trajectories, mean annual temperatures (with the annual harmonics and trend removed) at 150 m were generated from both model and observed data. The position of the 15°C at this depth was estimated from these distributions. These trajectories serve as the position of the GS as plotted on Figure 7.

[44] Between about 65°W and 45°W (65°W and 50°W) in the observations (model), the GS axis is oriented approximately in the zonal direction (Figure 7). Time-longitude plots of the anomalous position of the modeled and observed axis of the GS are given in Figure 8. *Joyce et al.* [2000] performed an empirical orthogonal function (EOF) analysis between about 75°W and 55°W of essentially the same data set and found that the GS migrated meridionally in phase in a 1000 km band.

[45] The simpler analytical technique we employed provides similar results to those of *Joyce et al.* [2000] in both space and time for the observations and in space for the model. For example, the amplitudes of the north-south

movements are approximately equivalent in both representations west of 50°W, about 100 km. In addition, the observed (modeled) GS motions are essentially in phase across the longitude band, 70°W to 49°W (70°W to 50°W). In contrast however, the model results indicate a greater increase in the amplitude of meridional GS movement to the east of 50°W than found in the observations (Figures 7 and 8).

[46] The zero crossings from the *Joyce et al.* [2000] time series (not shown) indicate that in spite of the different methods employed the changes in phase given in the paper by *Joyce et al.* [2000] are reproduced in the analysis used herein. Both records have a distinctly decadal character. In contrast, the modeled time series has an approximately 20-year periodicity particularly prior to 1960 (Figure 8).

[47] The SST changes in both the model and observations (not shown) are generally in phase with the GS migrations shown in Figure 8. The SST anomalies have amplitudes greater than 3.5°C in both the observations and model. Thus, a significant portion of the standard deviations in the vicinity of the simulated and observed GS in Figure 6 can be attributed to north-south motions of the Stream. Similar east-west migrations of the NAC (not shown) account for the northeast extension from the GS of the higher modeled and observed SST standard deviations in Figure 6.
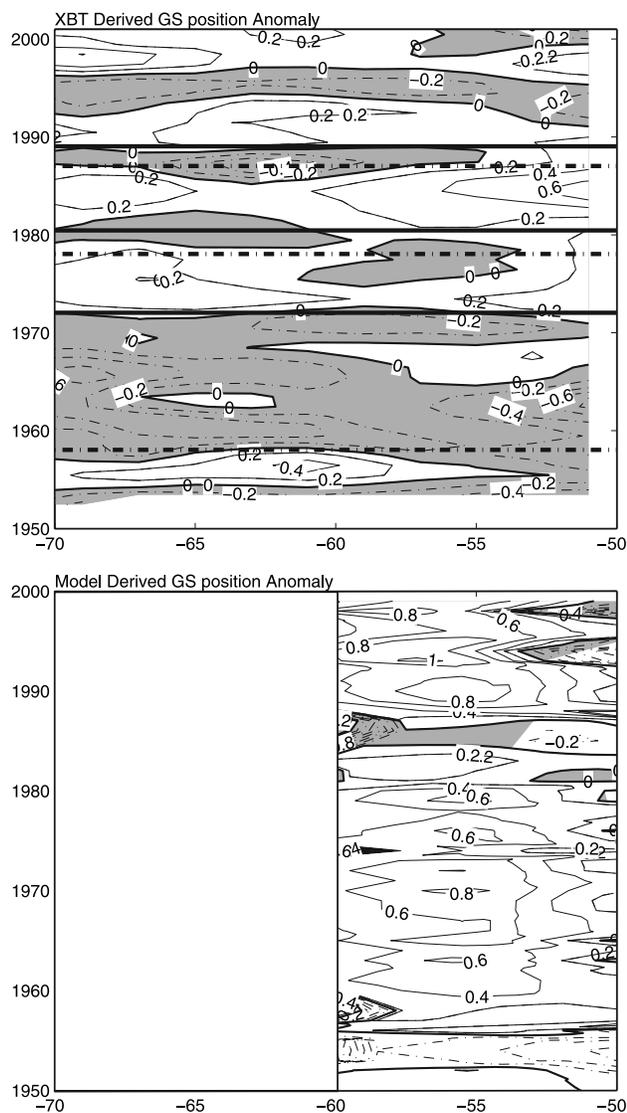
Figure 8. (top) Observed and (bottom) simulated time-longitude plot of the latitude of the 15°C (12°C) isotherm. The simulated section shown was chosen to represent the same position with respect to the location of the average axis of the Gulf Stream used by *Sutton and Allen* [1997]. Also shown are lines representing phase changes in the position of the stream from *Joyce et al.* [2000].

[48] Propagating decadal SST signals described by *Hansen and Bezdek* [1996], *Sutton and Allen* [1997] and *Sinha and Topliss* [2006] are another potential source of the larger standard deviations found along the GS and NAC paths (Figure 6). A trackline used to generate a time-distance plot located relative to the simulated GS consistent with the position of the *Sutton and Allen* [1997] section relative to the observed GS was constructed.

[49] *Sutton and Allen* [1997] show propagation along the entire length of their record, 1946 to 1989, until about 1970. However, signals starting in the Straits of Florida after about 1970 do no extend across the entire basin. *Sinha and Topliss* [2006] specifically comment on a similar change in the character of the propagating signals (i.e., signals generated after 1970 do not extend to the extreme eastern Atlantic as

do the earlier signals). There is no indication of anomaly propagation in the model results (Figure 9).

[50] In a previous section we noted that the simulated surface current distribution did not possess a southern GS recirculation gyre similar to observed. The westward flow that would mark the southern boundary of the recirculation gyre is found at 36°N (30°N) in the observations (simulation), Figure 1. However, the simulated temperature distribution at 150 m displays a recirculation gyre with similar properties to the observed feature (Figure 7).

4.5. Atlantic Multidecadal Oscillation (AMO)

[51] *Enfield et al.* [2001] defined an AMO index as a 10-year running mean of North Atlantic SST anomalies in a region extending from the equator to 70°N. They used an updated version of the monthly *Kaplan et al.* [1998] data set, which extends from 1856 to 1998. The resolution of this database is rather coarse, 5° in both latitude and longitude. The time series at each grid point were linearly detrended before calculating averages.

[52] The *Enfield et al.* [2001] AMO index includes two cycles of a signal with an approximately "65 to 80 year" period and peak to peak variability of about 0.4°C. We show all five SST time series for the North Atlantic from the model. The five curves are very similar in phase and amplitude suggesting that external forcing in the model at the longer periods exceeds the effects of internal oceanic variability. The model curves are similar to the observed AMO except for the first minima in the simulations, which leads the observed curve by about 20 years (Figure 10). *Knutson et al.* [2006] relate the 1880s model cooling to volcanic effects, which because of data paucity is not resolved by the limited observations. Additional analysis is required to determine if initial conditions can also contribute to the offset.

[53] To represent the spatial structure of the AMO, *Enfield et al.* [2001] computed and mapped correlations between their AMO index and the time series of SST at each 5° grid point. Similar correlation distributions were computed from the ERSST and CM2.1 results and the resulting spatial patterns are shown in Figure 11.

[54] The spatial distribution of AMO, SST correlations computed from the ERSST data is single signed throughout the North Atlantic (Figure 11) as in the paper by *Enfield et al.* [2001]. However, the same distribution estimated from the CM2.1 results has an area of small negative correlations located over and to the north of the model's GS. This area also is characterized by large SST standard deviation values (Figure 6). The presence of other large amplitude signals at different periods could serve to lower the correlations in this region.

4.6. The 1900–1999 Trends in SST

[55] As with the standard deviation computations described in the previous sections, (1) trends are computed from both model and observations for the period 1900–1999, and (2) the mean annual signal is removed from the grid point time series before trends are computed. In addition the trend from the control run for CM2.1, representative of the 1860 atmospheric composition, was subtracted from the model trend as in the paper by *Knutson et al.* [2006]. For consistency with previous comparisons we
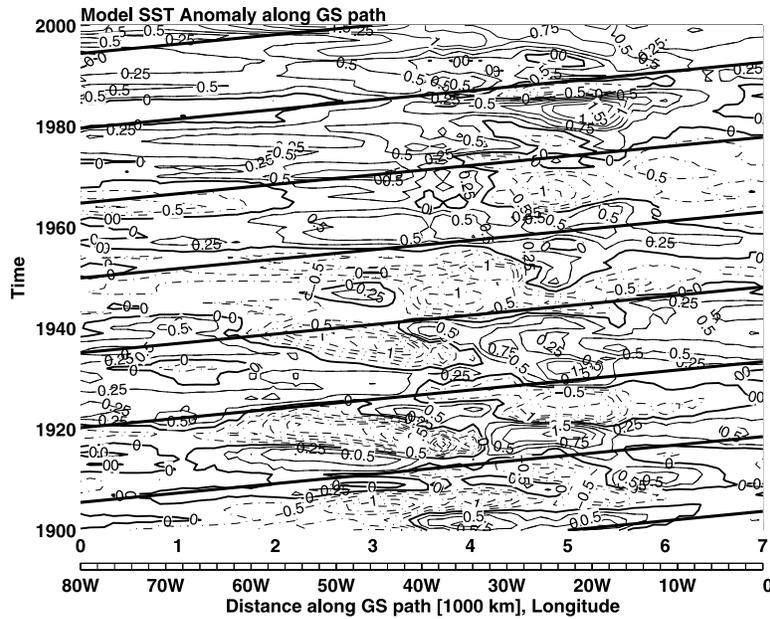
Figure 9. Time-longitude plot of simulated SST (°C). The simulated section was chosen to represent the same position with respect to the location of the average axis of the Gulf Stream used by *Sutton and Allen* [1997]. Also shown are phases representing the 1.7 cm/s phase speed of the anomalies estimated by *Sutton and Allen* [1997].

show one of the ensembles on Figure 12. Figure 12 also shows the average trend computed from the five ensembles.

[56] There are many difficulties in calculating trends such as selecting starting and end dates, amount of data available and quality of data. Thus we do not show differences

between the observed and simulated trends as performed for other parameters described. We will discuss the characteristics of the trend distributions.

[57] The average and one-ensemble member trend distributions are very similar. This should be expected from the
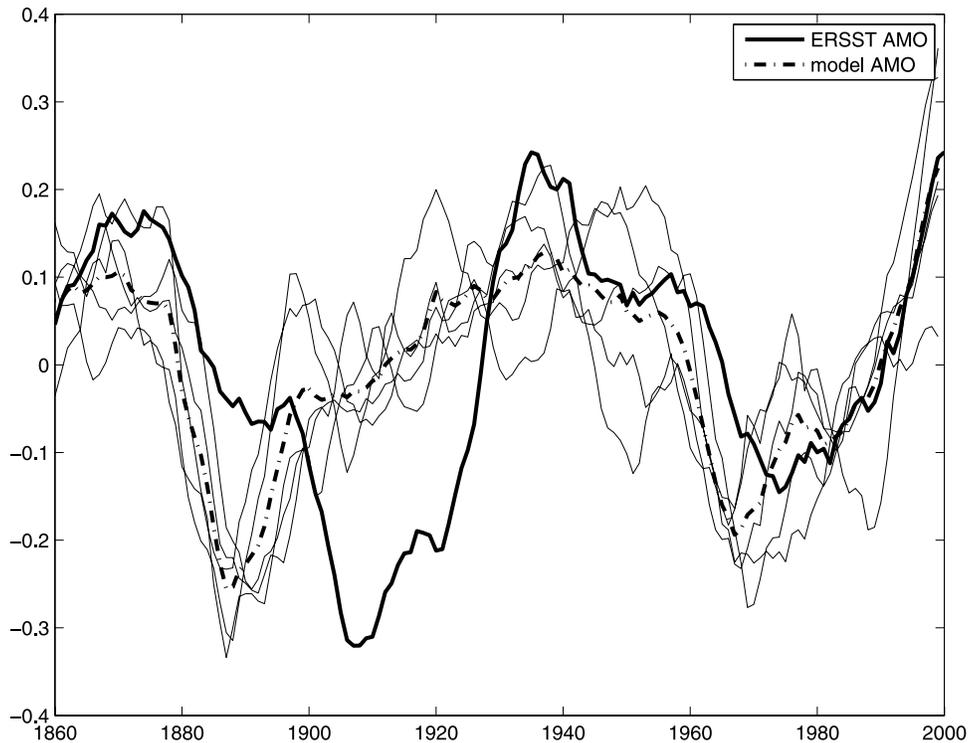

Figure 10. Observed (solid line), model average (dashed line), and the five-ensemble time series used to compute the average (light lines) of the average SST (°C) of the North Atlantic from the equator to 70°N. Each time series has been detrended and smoothed by a 10-year running mean filter.
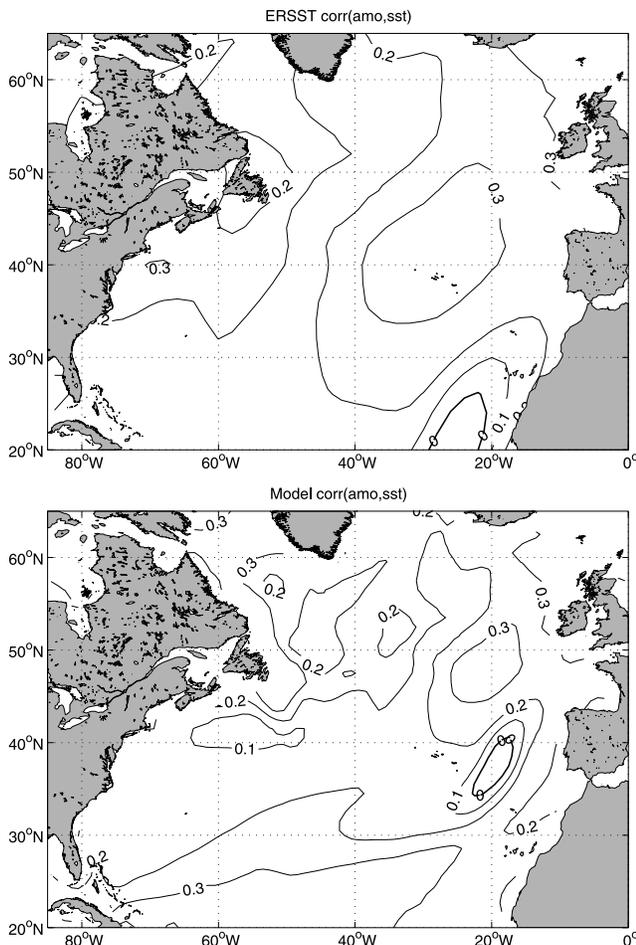
Figure 11. (top) Observed and (bottom) modeled spatial distribution of the correlation between the time series shown in Figure 10 and the time series of SST at each grid point.

similarities between the five-ensemble basin-wide SST time series shown in Figure 10. On the largest spatial scales the observed and simulated SST trend distributions for the 1900–1999 period are similar (Figure 12). In particular, the trends are characterized by positive values south of about 45°N and negative values to the north of this latitude.

[58] The *Knutson et al.* [2006] comparison of CM2.1 with the HADSST1 SST data of *Parker et al.* [1995] show similar results, specifically the negative trends south of Greenland in both simulations and observations. They go on to note that this is one of the few areas with cooling trends and that "the cooling trends in these regions generally do not appear to be statistically significant according to comparison with the control run 100-yr trends." However, the dipole pattern with a negative node south of Greenland appears in other modeling and observational studies (e.g., in observations at 100 m in the paper by *Harrison and Carson* [2007] and in observations and a model in the papers by both *Knutson et al.* [1999] (an older model than CM2.1) and *Karoly and Wu* [2005].

[59] However, there are differences in the SST trend distributions north of about 40°N. The simulated trend field (Figure 12) includes positive values greater than 0.5°C/century along the simulated axis of the GS (Figure 1) west of 40°W and along the axis of the modeled NAC between

50°N and 60°N and 30°W and 20°W. A simulated area of negative trends less than −0.5°C/century is found within the models surface representation of the western component of the subpolar gyre (Figure 12).

[60] The observed SST trend distribution has no maxima in the GS or NAC region (Figure 12). The simulated trend exhibits a maximum along the axis of GS with the largest value at about 40°N. The area of observed negative trend (≤.2°C/century) in the subpolar Atlantic also extends over a larger area than in the model, including not only the western portion of the subpolar gyre but also the eastern

5. Discussion

[61] Over most of the extratropical Atlantic, SSTs simulated by CM2.1 are within 1° of observed SST (Figure 1).

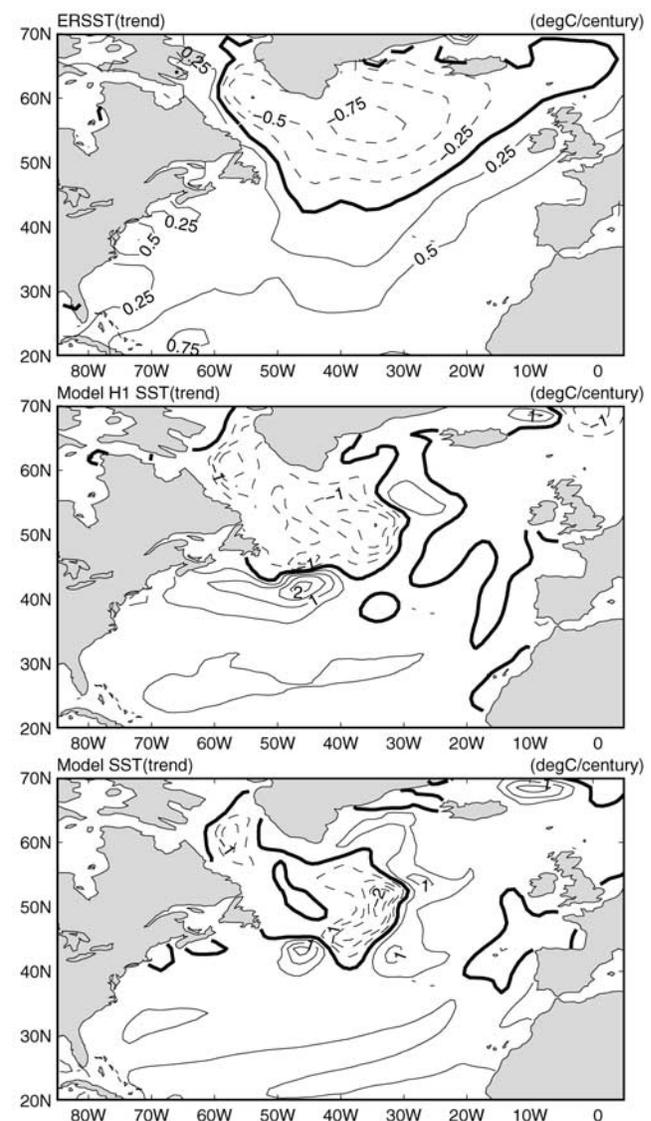**Figure 12.** Distribution of (top) observed and (middle) simulated trends (°C/century) computed for the 1900–1999 time series at each grid point. (bottom) Average trend distribution (°C/century) determined from the five ensemble members for the same time period.

Thus the model is capturing most of the large-scale characteristics of the SST structure of the subtropical and subpolar gyres. These successes are in part due to the many changes introduced in CM2.1 as reviewed by *Griffies et al.* [2005] and summarized in the papers by *Delworth et al.* [2006] and *Gnanadesikan et al.* [2006].

[62] However there are areas with differences greater than 2°C. As indicated by *Delworth et al.* [2006], the areas of larger differences are typically associated with strong mean currents. In addition there are discrepancies between many of the time-dependent signals. As stated earlier, we will concentrate on these large differences to identify areas for future study. We will also provide reasons for the importance of a particular region in prediction efforts.

5.1. Subtropical Gyre

[63] With respect to the mean subtropical gyre, as with most noneddy resolving models, the GS in CM2.1 separates at a more northerly latitude (~39°N) than observed (~37°N), Figure 2. The simulated GS remains some 100 km north of the observed current after separation. In addition, the model's LC does not turn anticyclonically around the Tail of the Grand Banks to provide colder subpolar waters to north of the GS in the same region. The northerly GS and the absence of an SC can both contribute to the higher model temperatures north of the GS. Previous studies have shown that increased spatial resolution can improve the ability of models to simulate both the separation latitude and location after separation of the axis of the GS [*Ozgokmen et al.*, 1997; *Chassignet and Garraffo*, 2001; *Maltrud and McClean*, 2003].

[64] If coupled models such as CM2.1 are eventually to be used in ecosystem forecasting it is important that they accurately simulate mean and time-dependent characteristics of the SC, north of the GS because of the observed effects of current changes on ecosystems. For example, *Greene and Pershing* [2003] describe two modal states for the waters along the shelf break north of the Stream. During the high (low) modal state there is reduced (increased) southward surface flow around the Grand Banks and the shelf break waters are warm (cold) and salty (fresh). The two states appear correlated with the North Atlantic Oscillation (NAO), with negative (positive) NAO phases associated with low (high) SC modal states.

[65] *Greene and Pershing* [2003] go on to note that these modal shifts are correlated with the distribution of sea life ranging from zooplankton to whales. During low modal states the cold and fresh westward flow from the Labrador Sea can penetrate "to the southwest as far as the Middle Atlantic Bight." Thus models must provide accurate simulations of the SC to ultimately be capable of accurate ecosystem forecasts in this region.

[66] The simulated GS extends considerably farther to the east than the observed GS before turning northeastward to become the NAC resulting in large temperature differences (Figure 1). *Roberts et al.* [1996] hypothesize that this difference is related to the formation of a nonexistent water mass formed in the subpolar gyre because of excessive mixing of overflow water and flux corrections applied in the model (a known shortcoming of level models). The artificial water mass tends to occupy space north of the GS thereby keeping the Stream at more southerly latitudes. There are no

flux corrections applied in CM2.1. However, erroneous surface fluxes generated in this coupled model could cause similar discrepancies. Incorrect simulation of overflows, e.g., if a nonexistent water mass is formed in CM2.1, could also contribute to the excessive eastward extension of the GS.

[67] Previously, we suggested that the absence of an Azores Current in CM2.1 could be related to the model's resolution. However, *Ozgokmen et al.* [2001], *Jia* [2000], and *Kida et al.* [2008], for example, find that Mediterranean outflow can cause the Azores Current. For instance, *Ozgokmen et al.* [2001] in a simple model study found that "the entrainment process associated with the Mediterranean outflow in the Gulf of Cadiz can impact the upper ocean circulation in the subtropical North Atlantic Ocean and can be a fundamental factor in the establishment of the Azores Current." Thus, the historical problem with level models of simulating accurately overflows might still be incompletely resolved.

[68] The greater than 2°C positive SST difference located between approximately 43°N and 53°N and 30°W and 20°W (Figure 1) occurs in a region were surface currents are weaker than those to the west in both representations and the flow directions are different. In the observations, the flow is essentially zonal; while in model the flow is southeastward representing a downstream extension of the NAC after it has made an anticyclonic turn. Thus, both NAC representations turn anticyclonically, but the former turns eastward and the latter curves southeastward (Figure 3).

[69] *Delworth et al.* [2006] find increased westerly winds compared to observations in this region in the CM2.1 simulation, which could cause increased southward Ekman transport in the model. This southward flow would advect lower temperatures from the north than would the observed westward flow. Heat budget calculations are needed to determine what proportion of the 2°C temperature discrepancy in this area is related to current differences, surface heat flux differences, mixing, etc.

[70] Time-dependent SST signals with decadal timescales have been associated with the northern edge of the subtropical gyre, as described previously. For instance, both the CM2.1 model and observations show that the GS migrates meridionally with an approximately 10-year cycle for the latter and 20-year cycle for the former (Figure 8).

[71] Changes in the meridional overturning circulation (MOC) have been given as possible causes of GS meridional motions. For instance, *Rossby and Benway* [2000] attribute "slow variations" in the GS path to "time-varying outflow of waters from the Labrador Shelf region," that is, an MOC process. *Joyce et al.* [2000] propose a similar mechanism based on differential export of Labrador Seawater and its effect on the Deep Western Boundary Current. The absence of continuity between the LC and SC in the model argues for a different mechanism for simulated decadal GS meridional motions than just given. *Joyce et al.* [2000] note that GS position is correlated with wintertime atmospheric storm paths. Thus, the difference in periodicities between model and observations must be resolved to use the former in long-term storm forecasting.

[72] Propagating SST signals represent another form of decadal SST variability associated with the GS/NAC. However, there is no indication of propagation of simulated SST

anomalies along the path selected for similitude with the path of *Sutton and Allen* [1997] during any portion of the model record (Figure 9). *Sutton and Allen* [1997] estimated a mean propagation speed for the SST anomalies they observed between 1945 and 1989 of 1.7 cm/s considerably less than the core speeds of the GS and NAC. Thus these signals have more complicated dynamics than pure advection by the strong currents.

[73] Two climate signals have been attributed to these propagating SST features. *Sutton and Allen* [1997] note that the propagating SST signals are correlated with propagating sea level pressure signals. In addition, *Sinha and Topliss* [2006] find that SST signals that do cross the entire Atlantic can have an impact on surface air temperatures of the United Kingdom. Thus both the GS movements and propagating SST signals need to be correctly simulated for accurate climate predictions for the North Atlantic.

5.2. Subpolar Gyre

[74] As noted previously, CM2.1 captures the main characteristics of the subpolar gyre; that is, the closed western gyre and the eastern northeastward flow that feeds the Norway Current. However, differences in the locations of various components of the subpolar gyre lead to large SST differences in the region. For example, as just described, in the west, the simulated GS extends considerably farther to the east than the observed flow (38°W versus 47°W) before turning northeastward to become the North Atlantic Current. The resulting displacement in the meridionally oriented SST contours associated with the NAC cause the greater than 4°C difference between observed and simulated centered at about 50°N, 40°W (Figure 1).

[75] Both the simulated and observed northward flowing IC represent extensions of the NAC. The observed IC is found to the east (~27°W to 23°W) of the simulated IC (~40°W to 35°W). The displacement between the two ICs causes the lower modeled temperatures (>2°C) centered at approximately 57°N, 35°W (Figure 12).

[76] The observed and simulated IC both turn cyclonically at about 65°N to flow southwestward alongside the EGC. Although the boundary flows in both representations are colocated along the boundary, there is a large unexplained temperature difference (+3°C) found here. The components of the subpolar gyre in the Labrador Sea, the LC and WGC, are associated with similar temperatures (Figure 1).

[77] On the eastern side of the subpolar gyre, the model fails to reproduce the intense flow in the center of the Iceland Basin. This portion of the subpolar gyre is the only intense current (e.g., IC, EGC, WGC, and LC) that does not flow along a continental slope. Its absence in the model may thus be related to the simulation's representation of the vertical density structure in the region.

[78] The pathway taken by water masses in the subpolar gyre determines, in part, the properties of water that is convected in the northern North Atlantic [e.g., *McCartney and Talley*, 1984] to return south in the Deep Western Boundary Current (i.e., water mass modification). Different pathways are likely to result in the water masses experiencing different surface heat flux and horizontal and vertical mixing patterns and thereby cause different degrees of water mass modification and effects on the MOC. For example, *Hatun et al.* [2005] find that changes in the dynamics of the

subpolar gyre can affect salinity input to the Arctic formation area of deep water masses that participate in the thermohaline circulation. Thus, accurate simulations of all the components of the subpolar gyre are necessary for accurate climate forecasts.

5.3. Basin-Wide Signals

[79] The coupled model CM2.1 simulates relatively accurately the spatial and temporal characteristics of the AMO at the surface of the North Atlantic (Figures 10 and 11). *Delworth and Mann* [2000], for example, have related longer-timescale SST signals such as the AMO to the MOC. Thus, additional model-data comparisons are warranted to determine if the coupled model also captures the spatial and temporal characteristics of the total water column AMO and MOC and potential climate impacts.

[80] For example, interest in the AMO has increased recently because of the findings of some studies suggest that the AMO has an impact on the number of tropical storms formed in the Atlantic. Specifically, *Goldenberg et al.* [2002] explain a dramatic increase in major hurricane activity between 1971 and 1994 and 1995–2000 to a change from a negative phase of the AMO to a positive phase. They go on to hypothesize that because of the multidecadal timescale of the AMO, increased formation of Atlantic tropical storms is likely to continue for several decades.

5.4. The 1900–1999 Trends in SST

[81] Both the modeled and observed trend distributions have a dipole-like character (Figure 12) similar to those of *Knutson et al.* [2006]. South (north) of 45°N, trends are generally positive (negative). *Häkkinen and Rhines* [2004] performed an EOF analysis on surface heat flux distributions in the Atlantic's subpolar gyre. They used data from a reanalysis of surface meteorological observations from the years 1978–2002. The first EOF had a dipole structure with heat loss (gain) over the subpolar (subtropical) gyre.

[82] The *Häkkinen and Rhines* [2004] record used to compute the EOFs is considerably shorter than the record used to compute the modeled and observed trends in Figure 12. However, their area of heat loss caused by surface heat fluxes approximately overlays the area of observed negative trend (i.e., it encompasses most of the subpolar North Atlantic) leading to the hypothesis that the observed and simulated trends are primarily caused by surface heat flux anomalies. Accurate simulations of the Atlantic trends are a critical requirement for the use of CM2.1 as a forecasting tool, particularly in the analysis of climate change.

5.5. Harmonics

[83] The model simulates the locations of largest amplitudes for both harmonics, which is coincident with the largest differences in the amplitudes of the harmonics. This area is along the eastern North American continent and is colocated with an area characterized by both net heat loss from the ocean to the atmosphere and large annual signal in net air-sea fluxes [*Isemer and Hasse*, 1987]. *Dong and Kelly* [2004] developed a simple thermodynamic three-dimensional model for this area. The model mixed layer temperature (i.e., SST) and mixed layer depth "show good agreement on seasonal and interannual time scales" with

observations and on these short timescales variability is primarily caused by heat flux anomalies. Thus, one possible cause for the large differences between observed and modeled ASAH and AAH could be erroneous simulations of surface fluxes in the coupled model.

[84] Finally, it is not obvious why the model simulates such large ASAH values in the extreme northern portion of the grid, Figure 4. The similarity of the observed results in Figures 4 and 5 with those generated by *Yashayaev and Zveryaev* [2001] suggest that the CM2.1 fields are valid. One possibility for the difference could be the manner in which the model simulates sea ice. The model's sea ice, particularly during March [*Delworth et al.*, 2006, Figure 14] extends farther south than observed and could contribute to differences between observed and simulated SST in the region. Since the annual harmonics represent the largest source of SST variability it is critical that forecast models simulate these properties accurately. Thus detailed heat budget studies using model results from this region are needed to resolve these differences.

References

Brambilla, E., and L. D. Talley (2006), Surface drifter exchange between the North Atlantic subtropical and subpolar gyres, *J. Geophys. Res.*, *111*, C07026, doi:10.1029/2005JC003146.

Bryan, F. O., C. W. Boning, and W. R. Holland (1995), On the midlatitude in a high-resolution model of the North Atlantic, *J. Phys. Oceanogr.*, *25*, 289–305, doi:10.1175/1520-0485(1995)025<0289:OTMCIA>2.0.CO;2

Chassignet, E. P., and Z. D. Garraffo (2001), Viscosity parameterization and the Gulf Stream separation, paper presented at Aha Huliko's Hawaiian Winter Workshop, Univ. of Hawaii, Honolulu, Hawaii, 15–19 Jan.

Covey, C., et al. (2000), The seasonal cycle in coupled ocean-atmosphere general circulation models, *Clim. Dyn.*, *16*, 775–787, doi:10.1007/s003820000081.

Delworth, T. L., and M. E. Mann (2000), Observed and simulated multidecadal variability in the Northern Hemisphere, *Clim. Dyn.*, *16*, 661–676, doi:10.1007/s003820000075.

Delworth, T. L., et al. (2006), GFDL's CM2 coupled climate models. Part I: Formulation and simulation characteristics, *J. Clim.*, *19*, 643–674, doi:10.1175/JCLI3629.1.

Dong, S., and K. A. Kelly (2004), Heat budget in the Gulf Stream region: The importance of heat storage and advection, *J. Phys. Oceanogr.*, *34*, 1214–1231, doi:10.1175/1520-0485(2004)034<1214:HBITGS>2.0.CO;2.

Enfield, D. B., A. M. Mestas-Nunez, and P. J. Trimble (2001), The Atlantic multi-decadal oscillation and its relation to rainfall and river flows in the continental U.S., *Geophys. Res. Lett.*, *28*, 2077–2080, doi:10.1029/2000GL012745.

Flatau, M. K., L. Talley, and P. N. Niiler (2003), The North Atlantic Oscillation, surface current velocities, and SST changes in the subpolar North Atlantic, *J. Clim.*, *16*, 2355–2369, doi:10.1175/2787.1.

Fratantoni, D. M. (2001), North Atlantic surface circulation during the 1990's observed with satellite-tracked drifters, *J. Geophys. Res.*, *106*, 22,067–22,093, doi:10.1029/2000JC000730.

Gnanadesikan, A., et al. (2006), GFDL's CM2 global coupled models. Part II: The baseline ocean simulation, *J. Phys. Oceanogr.*, *19*, 675–697.

Goldenberg, S. B., C. W. Landsea, A. M. Mestas-Nunez, and W. M. Gray (2002), The recent increase in Atlantic hurricane activity: Causes and implications, *Science*, *293*, 474–479, doi:10.1126/science.1060040.

Greene, C. H., and A. J. Pershing (2003), The flip side of the North Atlantic Oscillation and modal shifts in slope-water circulation patterns, *Limnol. Oceanogr. Methods*, *48*, 319–322.

Griffies, S. M., et al. (2005), Formulation of an ocean model for global climate simulations, *Ocean Sci.*, *1*, 45–79.

Häkkinen, S., and P. B. Rhines (2004), Decline of subpolar North Atlantic circulation during the 1990s, *Science*, *304*, 555–559, doi:10.1126/science.1094917.

Hansen, D. V., and H. F. Bezdek (1996), On the nature of decadal anomalies in North Atlantic sea surface temperature, *J. Geophys. Res.*, *101*, 8749–8758, doi:10.1029/95JC03841.

Harrison, D. E., and M. Carson (2007), Is the world ocean warming? Upper-ocean temperature trends: 1950–2000, *J. Phys. Oceanogr.*, *37*, 174–187, doi:10.1175/JPO3005.1.

Hatun, H., A. B. Sando, H. Drange, B. Hansen, and H. Valdimarsson (2005), Influence of the Atlantic subpolar gyre on the thermohaline circulation, *Science*, *309*, 1841–1846, doi:10.1126/science.1114777.

Isemer, H. J., and L. Hasse (1987), *The Bunker Climate Atlas of the North Atlantic Ocean*, vol. 2, *Air-Sea Interactions*, 252 pp., Springer, Berlin.

Jia, Y. (2000), Formation of an Azores Current due to Mediterranean overflow in a modeling study of the North Atlantic, *J. Phys. Oceanogr.*, *30*, 2342–2358, doi:10.1175/1520-0485(2000)030<2342:FOAACD>2.0.CO;2.

Joyce, T. M., C. Deser, and M. A. Spall (2000), The relation between decadal variability of subtropical mode water and the North Atlantic Oscillation, *J. Clim.*, *13*, 2550–2569, doi:10.1175/1520-0442(2000)013<2550:TRBDVO>2.0.CO;2.

Kaplan, A. M., A. Cane, Y. Kushnir, and A. C. Clement (1998), Analysis of global sea surface temperatures 1856–1998, *J. Geophys. Res.*, *103*, 18,567–18,589, doi:10.1029/97JC01736.

Karoly, D. J., and Q. Wu (2005), Detection of regional surface temperature trends, *J. Clim.*, *18*, 4337–4343, doi:10.1175/JCLI3565.1.

Kida, S., J. F. Price, and J. Yang (2008), The upper-oceanic response to overflows: A mechanism for the Azores Current, *J. Phys. Oceanogr.*, *38*, 880–895, doi:10.1175/2007JPO3750.1.

Knutson, T. R., T. L. Delworth, K. W. Dixon, and R. J. Stouffer (1999), Model assessment of regional surface temperature trends (1949–1997), *J. Geophys. Res.*, *104*, 30,981–30,996, doi:10.1029/1999JD900965.

Knutson, T. R., T. L. Delworth, K. W. Dixon, I. M. Held, J. Lu, V. Ramaswamy, M. D. Schwarzkopf, G. Stenchikov, and R. J. Stouffer (2006), Assessment of twentieth-century regional surface temperature trends using the GFDL CM2 coupled models, *J. Clim.*, *19*, 1624–1651, doi:10.1175/JCLI3709.1.

Lumpkin, R., and Z. Garraffo (2005), Evaluating the decomposition of tropical drifter observations, *J. Atmos. Oceanic Technol.*, *22*, 1403–1415, doi:10.1175/JTECH1793.1.

Maltrud, M. E., and H. McClean (2003), An eddy resolving global 1/10-degree ocean simulation, *Ocean Modell.*, *8*, 31–34, doi:10.1016/j.ocemod.2003.12.001.

McCartney, M. S., and L. D. Talley (1984), Warm-to-cold water conversion in the northern North Atlantic Ocean, *J. Phys. Oceanogr.*, *14*, 922–935, doi:10.1175/1520-0485(1984)014<0922:WTCWCI>2.0.CO;2.

Molinari, R. L. (2004), Annual and decadal variability in the western subtropical North Atlantic: Signal characteristics and sampling methodologies, *Prog. Oceanogr.*, *62*, 33–66, doi:10.1016/j.pocean.2004.07.002.

Ozgokmen, T. M., E. P. Chassignet, and A. M. Paiva (1997), Impact of wind forcing, bottom topography and inertia on midlatitude jet separation in a quasigeostrophic model, *J. Phys. Oceanogr.*, *27*, 2460–2476, doi:10.1175/1520-0485(1997)027<2460:IOWFBT>2.0.CO;2.

Ozgokmen, T. M., E. P. Chassignet, and C. G. H. Rooth (2001), On the connection between the Mediterranean Outflow and the Azores Current, *J. Phys. Oceanogr.*, *31*, 461–480, doi:10.1175/1520-0485(2001)031<0461:OTCBTM>2.0.CO;2.

Parker, D. E., C. K. Folland, and M. Jackson (1995), Marine surface temperature: Observed variations and data requirements, *Clim. Change*, *31*, 559–600, doi:10.1007/BF01095162.

Rayner, N. A., D. E. Parker, E. B. Harten, C. K. Folland, L. V. Alexander, E. C. Kent, A. Kaplan, and D. P. Powell (2003), Global analyses of sea surface temperature, sea ice and night marine air temperature since the late nineteenth century, *J. Geophys. Res.*, *108*(D14), 4407, doi:10.1029/2002JD002670.

Reverdin, G., P. P. Niiler, and H. Vladimarsson (2003), North Atlantic Ocean surface drifters, *J. Geophys. Res.*, *108*(C1), 3002, doi:10.1029/2001JC001020.

Roberts, M. J., R. March, A. L. New, and R. A. Wood (1996), An intercomparison of a Bryan-Cox type ocean model and an isopycnic model. Part I: The subpolar gyre and high latitude processes, *J. Phys. Oceanogr.*, *26*, 1495–1527.

Rossby, T., and R. W. Benway (2000), Slow variations in the mean path of the Gulf Stream east of Cape Hatteras, *Geophys. Res. Lett.*, *27*, 117–120, doi:10.1029/1999GL002356.

Sinha, B., and B. Topliss (2006), A description of interdecadal time-scale propagating North Atlantic sea surface temperature anomalies and their effect on winter European climate, 1948–2002, *J. Clim.*, *19*, 1067–1079, doi:10.1175/JCLI3646.1.

Smith, R. D., M. E. Maltrud, F. O. Bryan, and M. W. Hecht (2000), Numerical simulation of the North Atlantic Ocean at 1/10°, *J. Phys.*

Oceanogr., *30*, 1532–1561, doi:10.1175/1520-0485(2000)030<1532: NSOTNA>2.0.CO;2.

Smith, T. M., and R. W. Reynolds (2003), Extended reconstruction of global sea surface temperatures based on COADS data (1854–1997), *J. Clim.*, *16*, 1495–1510, doi:10.1175/1520-0442(2003)016<1495: EROGSS>2.0.CO;2.

Smith, T. M., and R. W. Reynolds (2004), Improved reconstruction of SST (1854–1997), *J. Clim.*, *17*, 2466–2477, doi:10.1175/1520-0442(2004)017<2466:IEROS>2.0.CO;2.

Sutton, R. T., and M. R. Allen (1997), Decadal predictability of North Atlantic sea surface temperature and climate, *Science*, *388*, 563–567.

Taylor, A. H., and J. A. Stephens (1998), The North Atlantic Oscillation and the latitude of the Gulf Stream, *Tellus, Ser. A*, *50*, 134–142.

Treguier, A. M., S. Theetten, E. P. Chassignet, T. Penduff, R. Smith, L. Talley, J. O. Beisman, and C. Boning (2005), The North Atlantic subpolar gyre in four high resolution models, *J. Phys. Oceanogr.*, *35*, 757–774, doi:10.1175/JPO2720.1.

Yashayaev, I. M., and I. I. Zveryaev (2001), Climate of the seasonal cycle in the North Pacific and the North Atlantic oceans, *Int. J. Climatol.*, *21*, 401–417, doi:10.1002/joc.585.

———————————

Z. Garraffo and R. L. Molinari, Rosenstiel School of Marine and Atmospheric Science, University of Miami, Coral Gables, FL 33124, USA. (bob.molinari@noaa.gov)

D. Snowden, Climate Project Office, Office of Climate Observations, National Oceanic and Atmospheric Administration, 1100 Wayne Avenue, Suite 1202, Silver Spring, MD 20910, USA.